Consistent estimates from satellites and models for the first aerosol indirect forcing

Joyce E. Penner,[1] Cheng Zhou,[1] and Li Xu[1]

Received 30 March 2012; revised 5 June 2012; accepted 13 June 2012; published 14 July 2012.

[1] Satellite-based estimates for the aerosol indirect forcing are consistently smaller than those from models due, in part, to the use of present-day results that do not capture the temporal changes between present day and pre-industrial conditions. Here, we use results from a coupled aerosol-climate model to pick regions and seasons that are sufficiently pristine to represent pre-industrial conditions. Then we use results from MODIS and CERES to estimate the forcing between present and pre-industrial conditions. The estimated forcing in the North Pacific Ocean region ranges from -1.8 to -2.2 Wm^{-2} from observations. This range is similar to our modeled forcing for this region, -2.65 Wm^{-2}, but is smaller than the modeled forcing using the same methodology as that used with the satellite observations, -3.6 W/m^2. Nevertheless, a previous estimate based on satellite observations was a factor of 10 smaller, -0.2 to -0.5 Wm^{-2}. Results demonstrate that while the estimated forcing from models may be somewhat larger than estimates based on satellite data, a judicious choice of analysis methods, yields results that are much closer than previous satellite and model-based comparisons. **Citation:** Penner, J. E., C. Zhou, and L. Xu (2012), Consistent estimates from satellites and models for the first aerosol indirect forcing, *Geophys. Res. Lett.*, *39*, L13810, doi:10.1029/2012GL051870.

1. Introduction

[2] The first aerosol indirect effect, or Twomey effect, is measured by the change in top of the atmosphere (TOA) solar fluxes caused by the change in cloud droplet number when cloud liquid water path and other morphological changes are held constant. Satellite measurements of cloud droplet number concentration (N_c) vs aerosol optical depth (τ_a) have been used to estimate the effect of changes in N_c due to anthropogenic aerosols and range from -0.2 Wm^{-2} to -0.5 Wm^{-2} [*Quaas et al.*, 2006, 2008]. In contrast, model results that rely on mechanistic descriptions of the relationship between aerosols and cloud drop number concentrations range from -0.5 Wm^{-2} to -1.85 Wm^{-2} but can be even larger, depending on how aerosol nucleation is treated in the model and whether a lower limit for droplet number concentrations is specified [*Lohmann and Feichter*, 2005; *Wang and Penner*, 2009].

[3] *Penner et al.* [2011a] used a model study to show that satellite-based estimates that rely on either the spatial variation of $\ln(N_c)$ vs $\ln(\tau_a)$ or $\ln(AI)$, where AI is the Aerosol Index (Ångström exponent times τ_a), rather than temporal variations induced by changes between the present (PD) and pre-industrial (PI) aerosol concentrations can significantly underestimate the Twomey effect.

[4] Here, we use model estimates of the average droplet number concentration and the regression between $\ln(N_c)$ and $\ln(AI)$ for both present-day and preindustrial results to choose regions for the present day that can act as a surrogate for pre-industrial conditions. Then satellite data are used to estimate the difference between present-day and preindustrial TOA fluxes. Unfortunately, among 14 regions examined, only the South Pacific Ocean (SPO) can be considered as a "pristine" surrogate for a few polluted regions, and then only during June, July, August (JJA) and December, January, February (DJF). When this region is used as a surrogate for PI conditions in DJF and JJA in the North Pacific Ocean (NPO), the TOA forcing from the satellite analysis is much closer to that estimated from the model.

2. Results

[5] We used the same 14 regions defined in *Quaas et al.* [2008] as well as data from all 4 seasons to estimate the predicted N_c and slope of the relationship between $\ln(N_c)$ and $\ln(AI)$ from PD and PI simulations. Our goal was to use the model results to find pristine regions and seasons in the Southern Hemisphere that could be used to describe the preindustrial values in the Northern Hemisphere. The response of N_c to increases in AI is expected to be a better indicator of aerosol/cloud interactions than is the response of N_c to τ_a [*Nakajima et al.*, 2001], so we focused on using these variables. *Wang et al.* [2009] have previously compared the predicted aerosol concentrations to data and *Wang and Penner* [2009] compared the model with droplet concentrations. *Quaas et al.* [2009] compared the slope of $\ln N_c$ with $\ln \tau_a$ from the model with satellite observations.

[6] All PI slopes for $\ln N_c$ vs $\ln AI$ and mean values of N_c differed significantly from PD values, except for the SPO region, where the difference in N_c between NPO PI DJF and JJA values and SPO PD JJA and DJF was less than 8%. The values of the slopes of $\ln N_c$ vs $\ln AI$ between the PD SPO and PI NPO were within 3% and a factor of 2 for NPO JJA and DJF, respectively (Table 1). Average τ_a and AI are also similar as well as the composition of the particles forming the cloud condensation nuclei concentrations (see auxiliary material).[1] Therefore, we judged this area as "pristine" and

[1]Department of Atmospheric, Oceanic, and Space Sciences, University of Michigan, Ann Arbor, Michigan, USA.

Corresponding author: J. E. Penner, Department of Atmospheric, Oceanic, and Space Sciences, Space Research Building, University of Michigan, 2455 Hayward St., Ann Arbor, MI 48109-2143, USA. (penner@umich.edu)

0094-8276/12/2012GL051870

[1]Auxiliary materials are available in the HTML. doi:10.1029/2012GL051870.

Table 1. Modeled Average Value of Droplet Number Concentrations, Aerosol Optical Depth (τ_a) and Index (AI), and Slope of the Change in Droplet Number With Aerosol Optical Depth or Aerosol Index in NPO and SPO[a]

	JJA for NPO; DJF for SPO				DJF for NPO; JJA for SPO			
	Average Droplet Number Concentration[b] (#/cm^3)	Average Aerosol Optical Properties[c] (τ_a, AI)	Slope of $\ln N_c$ vs $\ln \tau_a$[d]	Slope of $\ln N_c$ vs $\ln$AI[d]	Average Droplet Number Concentration[b] (#/cm^3)	Average Aerosol Optical Properties[c] (τ_a, AI)	Slope of $\ln N_c$ vs $\ln \tau_a$[d]	Slope of $\ln N_c$ vs $\ln$AI[d]
NPO PD	80.78 (70.17)	0.13 (0.06), 0.12 (0.07)	0.40 (0.91, 0.06)	0.51 (0.92, 0.06)	55.97 (64.29)	0.11 (0.08), 0.08 (0.09)	0.33 (0.74, 0.09)	0.47 (0.95, 0.04)
NPO PI	49.01 (39.70)	0.07 (0.03), 0.03 (0.02)	−0.002 (−0.04, 0.04)	0.32 (0.89, 0.05)	31.11 (26.17)	0.07 (0.02), 0.02 (0.01)	−0.07 (−0.39, 0.05)	0.39 (0.94, 0.04)
SPO PD	46.36 (42.46)	0.07 (0.04), 0.04 (0.02)	0.15 (0.55, 0.07)	0.65 (0.98, 0.04)	28.63 (32.38)	0.06 (0.03), 0.02 (0.01)	−0.001 (−0.01, 0.03)	0.38 (0.84, 0.07)

[a]Values are given for June, July, August (JJA) and December, January, February (DJF).
[b]The values in parentheses are standard deviation of the cloud droplet number concentration.
[c]The aerosol optical depth and aerosol index are separated by a comma. Standard deviations are in parentheses.
[d]The values in parentheses are the correlation coefficient and the margin of error for the 95% confidence level for the regression slope.

used SPO as a surrogate for pre-industrial conditions in NPO in the following. We note however that the slopes of $\ln N_c$ vs $\ln \tau_a$ differ in these regions, so in this sense the SPO is not "pristine".

[7] *Wang and Penner* [2009] describe the off-line radiative transfer calculation using N_c, leading to changes in cloud albedo and forcing. We used saved values of N_c and aerosol concentrations from the coupled aerosol/climate model [*Wang and Penner*, 2010], rather than the previously described off-line calculation of N_c, since the effects of sedimentation, precipitation and coagulation are present in the satellite data, so should be present in the model as well. Here, as in *Penner et al.* [2011a], we used monthly average aerosol concentrations together with 4-hourly meteorological fields at a $2^\circ \times 2.5^\circ$ resolution to estimate instantaneous aerosol optical depths and Ångström exponents as seen by satellites at the overpass time of 1:30 pm. Note that the use of hourly data does not alter our results significantly [*Penner et al.*, 2011b]. Estimates of the cloud albedo change and forcing based on these inline quantities of N_c used PD cloud fields (water vapor, water path and cloud fraction) to eliminate any feedback to cloud liquid water path (LWP) or cloud fraction (f) caused by changes in aerosols in the coupled aerosol/general circulation model.

[8] For satellite data we used the CERES SSF1deg Edition 2.6 data from 2002 to 2011 which provides $1 \times 1^\circ$ CERES-observed albedo estimates and coincident MODIS-derived f, LWP and cloud phase (available at http://ceres.larc.nasa.gov/products.php?product=SSF). Albedo estimates are based on instantaneous data, but since the satellite only sampled once per day, they are assumed to represent the average of this single value over the length of the day (details are available at http://ceres.larc.nasa.gov/documents/DQ_summaries/CERES_SSF1deg-lite_Ed2.6_DQS.pdf.)

[9] Figures 1a and 1b show a plot of the all-sky albedo for JJA in NPO and DJF in SPO (a similar figure showing DJF in NPO and JJA in SPO is available in the auxiliary material), while Table 2 shows average values for whole-sky, clear sky, and cloudy-sky albedos. The cloudy sky albedo is not directly available from satellite data, but can be estimated from

$$\alpha_{cld} = (\alpha - (1-f)\alpha_{clr})/f \quad (1)$$

where α and α_{clr} are the all-sky and clear sky albedos. There is clearly an increase in the all-sky NPO albedo compared to SPO, but this may be due to increases in cloud fraction, LWP, and aerosols in clear sky regions. Therefore, to avoid contamination by these factors, we first sorted the data using only those data with $f > 99\%$ (shown in Figures 1c and 1d), but also provide estimates for f > 50% (see Table 2). Then these albedo data were compiled into 10 LWP bins, evenly spaced in ln(LWP) intervals of 0.3 from 3 to 6 (with LWP in gm^{-2}). A test using up to 30 bins gave results similar to those reported here. Figure 2 shows a plot of ln (albedo) vs LWP for $f > 99\%$ together with the standard deviation of albedo within each LWP bin for NPO in JJA and SPO in DJF (Figure 2a) as well as for NPO in DJF and SPO in JJA (Figure 2b). The relative increase (%) for each LWP bin is also shown. While albedo clearly increases with LWP (Figures 2a and 2b) there is not any systematic difference in the percentage change between NPO and SPO with albedo (Figures 2c and 2d). On average, we find a change in albedo

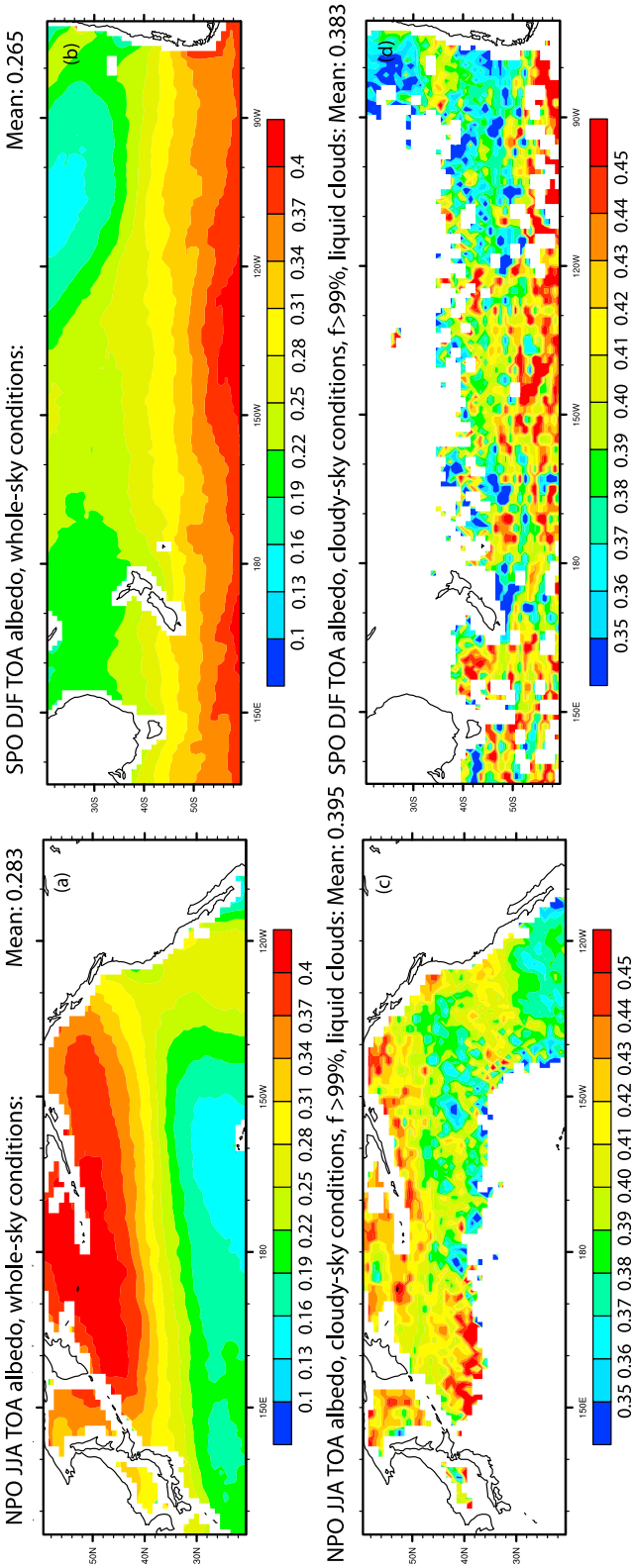

Figure 1. Albedo for all-sky conditions in (a) NPO JJA and (b) SPO DJF. Albedo for only those liquid clouds with f > 99% in (c) NPO JJA and (d) SPO DJF. Note the change in scale between Figures 1a and 1b and Figures 1c and 1d.

Table 2. Satellite and Model Albedos for All-Sky, Clear Sky and Cloudy Sky and for Liquid Clouds Using f > 99% and f > 50%

	All-Sky	Clear Sky	Cloudy Sky[a]	Cloudy Sky for Liquid Only Water Clouds, f > 99%[a]	Cloudy sky for Liquid Only Water Clouds, f > 50%[a]
Observation					
NPO JJA	0.283	0.089	0.357	0.395–0.397	0.339–0.340
SPO DJF	0.265	0.088	0.346	0.383–0.386	0.334–0.326
Difference (%)	6.36%	1.34%	3.08%	2.95%[b]	2.92%[b]
NPO DJF	0.367	0.159	0.428	0.483–0.472	0.441–0.390
SPO JJA	0.344	0.158	0.409	0.454–0.440	0.417–0.381
Difference (%)	6.27%	0.63%	4.44%	6.81%[b]	4.06%[b]
Model					
NPO JJA	0.342	0.070	0.474	0.490–0.482	0.479–0.465
NPO JJA PI	0.332	0.070	0.459	0.470–0.456	0.461–0.445
Difference (%)	3.03%	0.00%	3.25%	4.68%[b]	4.08%[b]
NPO DJF	0.376	0.137	0.562	0.586–0.584	0.562–0.550
NPO DJF PI	0.366	0.137	0.544	0.563–0.562	0.538–0.528
Difference (%)	2.55%	0.00%	3.05%	3.79%[b]	4.16%[b]

[a]Cloudy sky albedos are not directly available from satellite observations, but calculated from equation (1) summed over all grid boxes. Two values appear in the table. The first estimate was obtained by first averaging all values for a given spatial location over time, and then forming the spatial average, while the second was obtained by treating all values as equal when forming the average.
[b]The percentage change is based on the average percentage change for the 2 methods of averaging described in footnote a.

of 1.5% between JJA NPO and DJF SPO, whereas the increase is 4.4% in NPO DJF. The albedo change is 1.6% in NPO JJA and 2.7% in DJF if we use all data with $f > 50\%$.

[10] The observation-based forcing was calculated from the reflected solar fluxes in cloudy skies:

$$\Delta F = \left(\frac{\sum_{x,y} S_{0,x,y}\alpha_{x,y}A_{x,y}}{\sum_{x,y} A_{x,y}} - \frac{\sum_{x,y} S_{0,x,y}(1-f_{x,y})\alpha_{clr,x,y}A_{x,y}}{\sum_{x,y} A_{x,y}} \right) \Delta\alpha_{NPO-SPO}. \quad (2)$$

[11] Here, the first term is the all sky flux, while the second is the clear sky flux. The summation over x,y is taken over all grid boxes in a region. $S_{0,x,y}$ is the incoming solar radiation over each grid box, $f_{x,y}$ is the fraction of each grid box covered by clouds, $\alpha_{x,y}$ is the observed all sky albedo in each grid box, $\alpha_{clr,x,y}$ is the clear sky albedo, $\Delta\alpha_{NPO\text{-}SPO}$ is the average fractional change in albedo, and $A_{x,y}$ is the area of the grid box.

[12] Table 3 summarizes the observation-based forcing calculated using equation (2) from the satellite and the model. For model calculations based on equation (2), we replaced $\Delta\alpha_{NPO\text{-}SPO}$ with the average fractional change in cloudy sky albedo between PD and PI conditions in the NPO, but all other values were based on the observations. The estimated annual average forcing (average of JJA and DJF) for the observations ranges from -1.78 to -2.24 Wm^{-2} while that for the model ranges from -3.53 to -3.55 Wm^{-2}. The JJA results from the model are a factor of 2.3 to 2.7 higher than the observations, but the DJF model results are a factor of 1.6 larger (for $f > 50\%$) to 13% smaller (for $f > 99\%$). The primary reason for the model overestimate in JJA is the much larger change in τ_a between PD and PI results than that in the observations between NPO and SPO (see discussion in auxiliary material and Table S2).

[13] The model results based on equation (2) are on average larger than those from the satellite data, but they are much closer than the factor of 10 difference between the full model PD and PI estimates, -2.65 Wm^{-2} (shown as the last row in Table 3) and the values of $-0.2 \sim -0.5$ Wm^{-2} estimated for this region from satellites using methods that do not try to calibrate to "pristine" regions for PI estimates [*Quaas et al.*, 2008, Figure 5b]. Thus, we show that when applied in a judicious manner, satellite data give results for the first indirect forcing that are of the same order of magnitude as the results from a model.

3. Discussion

[14] We have shown previously that the use of satellite data for present day without consideration of temporal variations is subject to large errors [*Penner et al.*, 2011a, 2011b]. Here, we used data from the "pristine" South Pacific Ocean as a surrogate for pre-industrial conditions. When we do so, the satellite estimates of forcing for the NPO range from -1.8

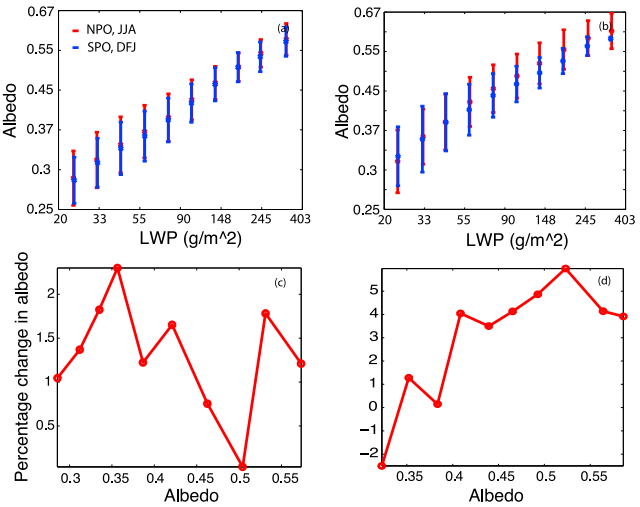

Figure 2. Measured albedo as a function of LWP for (a) NPO JJA and SPO DJF and (b) NPO DJF and SPO JJA for clouds with f > 99%. Error bars indicate the standard deviation. Percentage change in albedo between (c) NPO JJA and SPO DJF and (d) NPO DJF and SPO JJA.

Table 3. Estimates of Forcing (Wm^{-2}) in the NPO Region Between PD and PI From Satellite Observations and Model Results

	JJA, $f > 50\%$	JJA, $f > 99\%$	DJF, $f > 50\%$	DJF, $f > 99\%$
Observation-based forcing (equation (2))	−1.90	−1.77	−1.65	−2.71
Model-based forcing (equation (2)[a])	−4.41	−4.73	−2.64	−2.37
Model-based forcing from PD – PI results[b]	−4.13		−1.68	

[a]The model results in equation (2) use the regional average fractional change in albedo from the modeled PD and PI results for N_c together with the outgoing SW fluxes from the observations.

[b]The model-based forcing from PD-PI refers to the results calculated with the off-line radiative transfer model using the inline calculation N_c as in *Penner et al.* [2011a]. All cloud fractions are included.

to −2.2 Wm^{-2} while the corresponding results from the model using the same method of analysis range from −3.5 to −3.6 Wm^{-2}. Perhaps surprisingly, results from the full PD-PI off-line calculated forcing are even closer to the satellite results, −2.65 Wm^{-2}.

[15] To explain this result, we examined observed and modeled cloudy sky albedos and cloud fractions (Table S3 in the auxiliary material). The modeled cloud albedos are larger than the observed albedos, while the cloud fraction is much smaller. In JJA, the forcing based on the satellite observations is smaller than the modeled (PD-PI) forcing since the observed cloud fraction is only 7% larger, and the modeled τ_a difference is significantly larger than that in the observations (Table S2 in the auxiliary material). However, in DJF, the forcing from satellites is larger for the f > 99% case than the PD-PI modeled value, and similar for the f > 50% case, since the observed cloud fraction is 37% larger, even though the τ_a difference is similar (Table S3 in the auxiliary material). Thus, differences in LWP (as expressed in cloud albedos), cloud fraction, and aerosol optical depths lead to compensating differences that combine to produce a modeled PD and PI forcing that is close to that estimated from the observations.

[16] Our estimates for aerosol indirect forcing from observations are subject to several assumptions. First, we assumed that the SPO region could be used as a surrogate for PI conditions in the NPO region. Such an assumption has been made since the earliest attempts to gauge the effects of aerosols on clouds [e.g., *Schwartz*, 1988]. However, we tested the use of the SPO region by comparing model results for PI cloud and aerosol properties in the NPO with those from the PD SPO. Second, we assumed that ice clouds did not mask the change in outgoing shortwave radiation caused by changes in warm-phase clouds. This assumption can be tested by comparing the forcing in the model with and without ice-clouds included. When we do so, the estimated forcing is reduced by about 10%. Also, we assumed that the meteorological conditions leading to a change in albedo at a fixed LWP were similar in the NPO and SPO. Cloud resolving model studies have shown that the response of clouds to increasing aerosols depends in large part on the meteorological conditions or the specified large-scale forcing [e.g., *Ackerman et al.*, 2004; *Guo et al.*, 2007]. But these model results include both the first indirect forcing (or albedo effect) as well as the response of LWP and cloud fraction to changes in aerosols. Our methodology avoids including these responses. Finally we assumed that the fractional increase in cloud albedo for liquid water clouds is the same for all cloud fractions. This is perhaps the most limiting assumption in our study. Our study selects conditions that only include clouds that cover at least 50% of a $1^\circ \times 1^\circ$ grid, but estimates the forcing assuming that the fractional response of the cloud albedo for the first indirect effect for all cloud fractions is similar. This assumption should be approximately followed for the *initial* cloud droplet concentrations as long as the updrafts that determine the initial cloud drop change do not depend on the meteorological conditions that determine the cloud fraction, and as long as the mixing of cloud air with clear air is similar for all cloud fractions (i.e. the clouds are heterogeneously mixed to the same degree for all cloud fractions). Both assumptions can call our observational estimates into question. Indeed, since global model estimates of albedo effects often make these same assumptions, it is perhaps not surprising that the results from the model and that from observations using our method are similar. Still, it is comforting that if one adds such qualifications to the observational analysis, the results of the model and the observations are within a factor of two.

[17] **Acknowledgments.** The NCAR CISL provided computer time for this study. We thank both reviewers for suggestions that improved the manuscript.

[18] The Editor thanks two anonymous reviewers for their assistance in evaluating this paper.

References

Ackerman, A. S., M. P. Kirkpatrick, D. E. Stevens, and O. B. Toon (2004), The impact of humidity above stratiform clouds on indirect aerosol climate forcing, *Nature*, *432*, 1014–1017, doi:10.1038/nature03174.

Guo, H., J. E. Penner, M. Herzog, H. Pawlowska (2007), Examination of the aerosol indirect effect under contrasting environments during the ACE-2 experiment, *Atmos. Chem. Phys.*, *7*, 535–548, doi:10.5194/acp-7-535-2007.

Lohmann, U., and J. Feichter (2005), Global indirect aerosol effects: A review, *Atmos. Chem. Phys.*, *5*, 715–737, doi:10.5194/acp-5-715-2005.

Nakajima, T., A. Higurashi, K. Kawamoto, and J. E. Penner (2001), A possible correlation between satellite-derived cloud and aerosol microphysical parameters, *Geophys. Res. Lett.*, *28*, 1171–1174, doi:10.1029/2000GL012186.

Penner, J. E., L. Xu, and M. Wang (2011a), Satellite methods underestimate indirect climate forcing by aerosols, *Proc. Natl. Acad. Sci. U. S. A.*, *108*, 13,404–13,408, doi:10.1073/pnas.1018526108.

Penner, J. E., C. Zhou, L. Xu, and M. Wang (2011b), Reply to Quaas et al.: Can satellites be used to estimate indirect climate forcing by aerosols?, *Proc. Nat. Acad. Sci. U. S. A.*, *108*, E1100–E1101.

Quaas, J., O. Boucher, and U. Lohmann (2006), Constraining the total aerosol indirect effect in the LMDZ and ECHAM4 GCMs using MODIS satellite data, *Atmos. Chem. Phys.*, *6*, 947–955, doi:10.5194/acp-6-947-2006.

Quaas, J., O. Boucher, N. Bellouin, and S. Kinne (2008), Satellite-based estimate of the direct and indirect aerosol climate forcing, *J. Geophys. Res.*, *113*, D05204, doi:10.1029/2007JD008962.

Quaas, J., et al. (2009), Aerosol indirect effects: General circulation model intercomparison and evaluation with satellite data, *Atmos. Chem. Phys.*, *9*, 8697–8717, doi:10.5194/acp-9-8697-2009.

Schwartz, S. E. (1988), Are global cloud albedo and climate controlled by marine phytoplankton?, *Nature*, *336*, 441–445, doi:10.1038/336441a0.

Wang, M., and J. E. Penner (2009), Aerosol indirect forcing in a global model with particle nucleation, *Atmos. Chem. Phys.*, *9*, 239–260, doi:10.5194/acp-9-239-2009.

Wang, M., and J. E. Penner (2010), Cirrus clouds in a global climate model with a statistical cirrus cloud scheme, *Atmos. Chem. Phys.*, *10*, 5449–5474, doi:10.5194/acp-10-5449-2010.

Wang, M., J. E. Penner, and X. Liu (2009), Coupled IMPACT aerosol and NCAR CAM3 model: Evaluation of predicted aerosol number and size distribution, *J. Geophys. Res.*, *114*, D06302, doi:10.1029/2008JD010459.